
Multimodal Imaging of 2-Cycle PRRT with ^{177}Lu -DOTA-JR11 and ^{177}Lu -DOTATOC in an Orthotopic Neuroendocrine Xenograft Tumor Mouse Model

Jakob Albrecht^{1–3}, Samantha Exner⁴, Carsten Grötzing^{2–4}, Sonal Prasad^{1,5}, Frank Konietschke^{6,7}, Nicola Beindorff⁵, Anja A. Kühl⁸, Vikas Prasad^{1,9}, Winfried Brenner^{1,2,5}, and Eva J. Koziol^{1–3}

¹Department of Nuclear Medicine, Charité–Universitätsmedizin Berlin, Berlin, Germany; ²German Cancer Consortium, Berlin, Germany; ³German Cancer Research Center, Heidelberg, Germany; ⁴Department of Hepatology and Gastroenterology, Charité–Universitätsmedizin Berlin, Berlin, Germany; ⁵Berlin Experimental Radionuclide Imaging Center, Charité–Universitätsmedizin Berlin, Berlin, Germany; ⁶Institute of Biometry and Clinical Epidemiology, Charité–Universitätsmedizin Berlin, Berlin, Germany; ⁷Berlin Institute of Health, Berlin, Germany; ⁸iPATH.Berlin–Immunopathology for Experimental Models, Charité–Universitätsmedizin Berlin; and ⁹Department of Nuclear Medicine, University Hospital Ulm, Ulm, Germany

Peptide receptor radionuclide therapy (PRRT) using radiolabeled somatostatin receptor (SSTR) analogs is a common approach in advanced neuroendocrine neoplasms. Recently, SSTR antagonists have shown promising results for imaging and therapy due to a higher number of binding sites than in commonly used agonists. We evaluated PRRT with SSTR agonist ^{177}Lu -DOTATOC and antagonist ^{177}Lu -DOTA-JR11 longitudinally in an orthotopic murine pancreatic neuroendocrine neoplasm model expressing human SSTR2. Morphologic and metabolic changes during treatment were assessed using multimodal imaging, including hybrid PET/MRI and SPECT/CT. **Methods:** In vitro radioligand binding and internalization assays and cell-cycle analysis were performed. SSTR2-transfected BON cells (BON-SSTR2) were used for in vivo experiments. Tumor-bearing mice received 2 intravenous injections of 100 μL of saline, 30 MBq of ^{177}Lu -DOTATOC, or 20 MBq of ^{177}Lu -DOTA-JR11 with an interval of 3 wk. Weekly T2-weighted MRI was performed for tumor monitoring. Viability of the tumor tissue was assessed by ^{18}F -FDG PET/MRI once after PRRT. Tumor and kidney uptake of the respective radiopharmaceuticals was measured 24 h after injection by SPECT/CT. **Results:** Compared with ^{177}Lu -DOTATOC, ^{177}Lu -DOTA-JR11 treatment resulted in an increased accumulation of cells in G2/M phase. Animals treated with the SSTR antagonist showed a significant reduction in tumor size ($P < 0.001$) and an increased median survival (207 d; interquartile range [IQR], 132–228) compared with ^{177}Lu -DOTATOC (126 d; IQR, 118–129). SPECT/CT revealed a 4-fold higher median tumor uptake for the antagonist and a 3-fold higher tumor-to-kidney ratio in the first treatment cycle. During the second therapy cycle, tumor uptake of ^{177}Lu -DOTATOC was significantly lower ($P = 0.01$) whereas ^{177}Lu -DOTA-JR11 uptake remained stable. Imaging of tumor morphology indicated comparatively larger necrotic fractions for ^{177}Lu -DOTA-JR11 despite further tumor growth. These results were confirmed by ^{18}F -FDG PET, revealing the least amount of viable tumor tissue in ^{177}Lu -DOTA-JR11-treated animals, at 6.2% (IQR, 2%–23%). **Conclusion:** ^{177}Lu -DOTA-JR11 showed a higher tumor-to-kidney ratio and a more pronounced cytotoxic effect than did ^{177}Lu -DOTATOC. Additionally, tumor uptake was more stable over the course of 2 treatment cycles.

Key Words: ^{177}Lu -DOTA-JR11; multimodal imaging; PET/MRI; somatostatin receptor antagonist; peptide receptor radionuclide therapy; SPECT/CT

J Nucl Med 2021; 62:393–398

DOI: 10.2967/jnumed.120.250274

A hallmark of most neuroendocrine neoplasms (NENs) is the overexpression of somatostatin receptors (SSTRs) on the tumor cell surface—a characteristic that has been extensively used for both diagnostic and therapeutic purposes. The current, well-established, therapy is based on targeting SSTR by peptide receptor radionuclide therapy (PRRT) (1).

Presently, PRRT for NEN is performed with SSTR agonists primarily targeting SSTR2, such as ^{177}Lu -DOTATATE (1,2) or ^{177}Lu -DOTATOC, which, in contrast to DOTATATE, also shows an additional low affinity for SSTR5. An improved quality of life and prolonged progression-free survival compared with nonradiolabeled SSTR analogs has been reported (3). In 2006, Ginj et al. were the first to point out the potential of SSTR antagonists for diagnostic and therapeutic purposes (4). SSTR antagonists recognize a higher number of receptor binding sites per cell, resulting in higher tumor-to-organ ratios than are possible with agonists (5–8). In a biodistribution study, a tumor-to-kidney ratio of 5.4 was reported for ^{177}Lu -DOTA-JR11, compared with 3.8 for ^{177}Lu -DOTATE, at 72 h after injection (8).

So far, few preclinical and clinical studies on PRRT using the antagonist ^{177}Lu -DOTA-JR11 have been published (8–12). Dalm et al. showed higher tumor uptake and significantly more DNA double-strand breaks for the SSTR antagonist in vitro (9). Longer tumor residence times and, thus, higher tumor radiation doses were reported in 2 clinical trials (7,12). However, little is known about treatment effects on the tumor itself as detectable by hybrid imaging.

The aim of this study was to compare the treatment effects of 2 cycles of ^{177}Lu -DOTATOC and ^{177}Lu -DOTA-JR11 in NENs and provide an imaging-based tumor response analysis. Using a murine orthotopic, SSTR2-positive pancreatic NEN model, we monitored treatment response longitudinally by multimodal imaging: tumor size and morphology by MRI, radionuclide uptake by SPECT/CT after each

Received May 27, 2020; revision accepted Jul. 9, 2020.
For correspondence or reprints contact: Winfried Brenner, Charité–Universitätsmedizin Berlin, Augustenburger Platz 1, 13353 Berlin, Germany.
E-mail: winfried.brenner@charite.de
Published online Aug. 28, 2020.
COPYRIGHT © 2021 by the Society of Nuclear Medicine and Molecular Imaging.

therapeutic injection, and ^{18}F -FDG PET to provide metabolic information.

MATERIALS AND METHODS

Cell Lines

Human pancreatic BON cells, a kind gift from Courtney M. Townsend (University of Texas, Galveston), were grown in RPMI 1640 medium (10% fetal calf serum, 1% penicillin/streptomycin) in a humidified atmosphere at 37°C with 5% CO_2 .

Native BON cells were transfected with human SSTR2 (BON-SSTR2) (pcDNA3.1-huSSTR2, #SSTR200000; cDNA Resource Center) as described by Exner et al. (13). Stable clones were validated for SSTR2 expression by quantitative real-time polymerase chain reaction, immunofluorescence, and radioligand binding assay (13).

Radiolabeling

The precursor DOTA-JR11 was kindly provided by Helmut Maecke (Freiburg, Germany), and DOTATOC was purchased from ABX GmbH. $^{177}\text{LuCl}_3$ and reagent kits were purchased from ITG Isotope Technologies. The radiopharmaceutical ^{177}Lu -DOTATOC was synthesized using reagent kits for ^{177}Lu manual labeling as per the manufacturer's protocol. DOTA-JR11 was radiolabeled with ^{177}Lu as follows: DOTA-JR11 (25 μg) dissolved in ascorbate buffer (500 μL) was added to $^{177}\text{LuCl}_3$ (1 GBq) and heated for 30 min at 95°C . After cooling to room temperature, the reaction was diluted with 1 mL of normal saline. Before intravenous injection, the pH of the tracer was adjusted to 6.0 using NaHCO_3 . A reverse-phase radio-high-performance liquid chromatography system (Knauer GmbH) was used for quality control. The radiochemical purities of ^{177}Lu -DOTATOC and ^{177}Lu -DOTA-JR11 were at least 99% and 95%–98%, respectively. The radiochemical yields of ^{177}Lu -DOTATOC and ^{177}Lu -DOTA-JR11 were 97%–99% and 90%–92%, respectively, and the respective specific molar activities were calculated as 44–50 and 21 GBq/ μmol .

Binding and Internalization Assays

Peptide iodination and binding assays with iodine-labeled somatostatin were performed as previously described (13); for receptor competition, increasing concentrations of unlabeled DOTATOC and DOTA-JR11 were used. Data were analyzed with GraphPad Prism, version 5.04, and half-maximal inhibitory concentration (IC_{50}) was calculated by nonlinear regression (1-site-fit $\log\text{IC}_{50}$, least-squares fit).

Internalization with ^{177}Lu -labeled somatostatin analogs was performed as previously described (9).

Cell-Cycle Analysis

Cell-cycle analysis was performed as previously described (13). The cells were treated with the indicated activities of ^{177}Lu -coupled somatostatin analogs for 4 h, washed, and incubated in fresh growth medium for a further 20 h before analysis.

Generation of Tumor Xenograft Models

All animal experiments were performed in accordance with national and local guidelines for animal welfare and were approved by the Berlin State Department for Health and Social Affairs (regulation G0011/16).

To generate the pancreatic tumor xenograft model, female severe combined immunodeficient mice were orthotopically inoculated with BON-SSTR2 cells. The surgery was performed under perioperative anesthesia and analgesia (ketamine, 0.06 mg/g intraperitoneally; metamizole, 0.2 mg/g; and carprofen, 0.005 mg/g subcutaneously) and inhalation anesthesia (1%–2% isoflurane in oxygen). A median laparotomy of 1–2 cm was performed, and 2.0 – 2.2×10^6 BON-SSTR2 cells in a volume of 20 μL (serum-free RPMI 1640) were inoculated directly into the pancreas tail using a 29-gauge syringe. To prevent leakage of tumor cells into the abdominal cavity, 0.04% polihexanide in Ringer solution was applied to the injection site with a cotton tip.

All animals were maintained under pathogen-free conditions and were fed with sterile food and water ad libitum. Animal weight was monitored once a week before the first therapeutic injection and twice per week after therapy started.

Preliminary Study

A preliminary study was performed to evaluate the activity used for PRRT in mice as reported in the current literature (9). Once tumors exceeded 100 mm^3 , animals with orthotopic pancreatic NENs received a single therapeutic intravenous 30-MBq injection of either ^{177}Lu -DOTA-JR11 ($n = 4$) or ^{177}Lu -DOTATOC ($n = 4$). The animals were monitored weekly by T2-weighted MRI until the tumors reached 1,000 mm^3 or body weight decreased by 20%.

PRRT

Each animal received 2 intravenous injections of 30 MBq of ^{177}Lu -DOTATOC ($n = 4$), 100 μL of sterile saline ($n = 4$), or 20 MBq of ^{177}Lu -DOTA-JR11 ($n = 4$). Because we observed severe toxicity in our preliminary study after administration of 30 MBq of ^{177}Lu -DOTA-JR11, the activity was reduced by 30%. ^{177}Lu -DOTATOC was used for reasons relating to the patent for ^{177}Lu -DOTATATE. The 2 treatment cycles were applied within a 3-wk interval, starting once the tumors exceeded approximately 80 mm^3 . Tumors were continuously monitored, and animals were euthanized once the tumors reached 1,000 mm^3 or body weight decreased by 20%.

In Vivo Imaging

For in vivo PET/MRI (nanoScan PET/MRI; Mediso) and SPECT/CT (nanoScan SPECT/CT; Mediso), the mice were anesthetized with 1%–2% isoflurane in oxygen. Body temperature was kept at 37°C using a heated bed aperture, and respiration rate was continuously monitored.

To assess tumor size and morphology, MRI scans were acquired using a T2-weighted fast spin-echo sequence as previously described (14).

To analyze metabolic tumor activity, ^{18}F -FDG PET/MRI was performed once when significant regrowth (tumor volume $> 700 \text{mm}^3$) was observed after the second treatment cycle. For ^{18}F -FDG PET, 10–20 MBq of ^{18}F -FDG were administered intravenously 37–60 min before a 30-min acquisition. A material map for attenuation correction and additional T2-weighted MRI were acquired.

To assess intratumoral uptake of ^{177}Lu -DOTATOC or ^{177}Lu -DOTA-JR11 during each therapy cycle, SPECT/CT was performed. A helical CT scan was acquired for anatomic orientation of the SPECT images.

Image Analysis

Interview Fusion software, version 3.01 (Mediso), was used to assess tumors. A tumor volume of interest was drawn manually on T2-weighted images for calculation of volumes.

PET and SPECT images were analyzed with PMOD, version 3.505 (PMOD Technologies Ltd.). For calculation of tumor and organ uptake, a volume of interest was placed over the whole tumor or organ on SPECT images, and the percentage uptake of the injected activity per milliliter was calculated. Because uptake was similar in the left and right kidneys, a mean value was calculated for both kidneys.

Metabolically active tumor tissue was determined by fused ^{18}F -FDG PET and T2-weighted MRI as previously described (15). Briefly, a tumor volume of interest was placed onto T2-weighted images. ^{18}F -FDG-avid tumor was automatically delineated by PMOD, using a threshold of 30% of the maximum activity within this volume. Viable tumor was defined as the ^{18}F -FDG-avid portion of the whole tumor volume as delineated in T2-weighted images.

Histopathology

Paraffin sections of tumor tissues were deparaffinized and stained with hematoxylin (Merck) and eosin (Sigma-Aldrich) as described elsewhere (16).

Statistics

Tumor growth delay was defined as the difference in time to reach a tumor volume of 1,000 mm³ between the treatment and control groups, as previously described (9). Linear interpolation was performed in MATLAB, version R2018a (MathWorks), to calculate the median tumor sizes per time point for each group. Because of the rather small sample sizes, approximate statistical methods for the analysis of factorial longitudinal data (repeated-measures designs) with factors “group” and “time” were used (17). The methods are implemented in the R package MANOVA.RM (18). For size comparison, both semiparametric (MANOVA.RM) and purely nonparametric (nparLD) (19) approaches for repeated-measures design were applied. All statistical analysis was performed using R software (version 3.6.1) at a 5% level of significance. Because of the very small sample sizes, *P* values are interpreted in an exploratory supplementary manner.

RESULTS

In Vitro

For assessing the therapeutic effects of ¹⁷⁷Lu-DOTATOC and ¹⁷⁷Lu-DOTA-JR11 in vitro, both tracers were applied to BON-SSTR2 cells. Strong binding was demonstrated for both tracers in a radioligand competition assay, and iodine-labeled somatostatin was displaced dose-dependently by unlabeled DOTATOC (IC₅₀, 13.1 nM) and DOTA-JR11 (IC₅₀, 2.3 nM), revealing a 6-fold higher affinity for the SSTR antagonist. Native BON cells reached only background levels of binding (Fig. 1A). Interestingly, the activity bound to BON-SSTR2

cells was up to 10-fold higher for antagonistic ¹⁷⁷Lu-DOTA-JR11 than for agonistic ¹⁷⁷Lu-DOTATOC. The largest fraction of the antagonist was membrane-bound (80% of cell-bound activity), whereas 80% of the agonist was internalized. As expected, native BON cells demonstrated only little binding, with no displacement (Fig. 1B).

For assessment of radiation effects on BON-SSTR2 cell proliferation, the cell-cycle distribution after incubation with either radioreceptor was analyzed. Cell-cycle phases remained unchanged in both BON-SSTR2 and BON cells after treatment with 0.1 or 1.0 MBq of ¹⁷⁷Lu-DOTATOC. In contrast, ¹⁷⁷Lu-DOTA-JR11 induced an increasing accumulation of BON-SSTR2 cells in G2/M, from 23% (control) to 38% (0.1 MBq) and 63% (1.0 MBq). This increase was mirrored by a decreased proportion of cells in G0/G1 phase (57% vs. 43% [0.1 MBq] or 17% [1.0 MBq]). Native BON cells showed no change in cell-cycle phases (Fig. 1C).

Preliminary Study

All animals receiving 30 MBq of ¹⁷⁷Lu-DOTA-JR11 died within 3 wk after PRRT, indicating severe toxicity from the administered activity. A significant weight loss was observed before death. Post-mortem dissection did not reveal any signs of internal bleeding, infection, or other obvious causes of death.

¹⁷⁷Lu-DOTATOC-treated animals tolerated the 30-MBq activity well, and T2-weighted MRI revealed a stable tumor size for 3 wk (Supplemental Fig. 1; supplemental materials are available at <http://jnm.snmjournals.org>) before tumor regrowth.

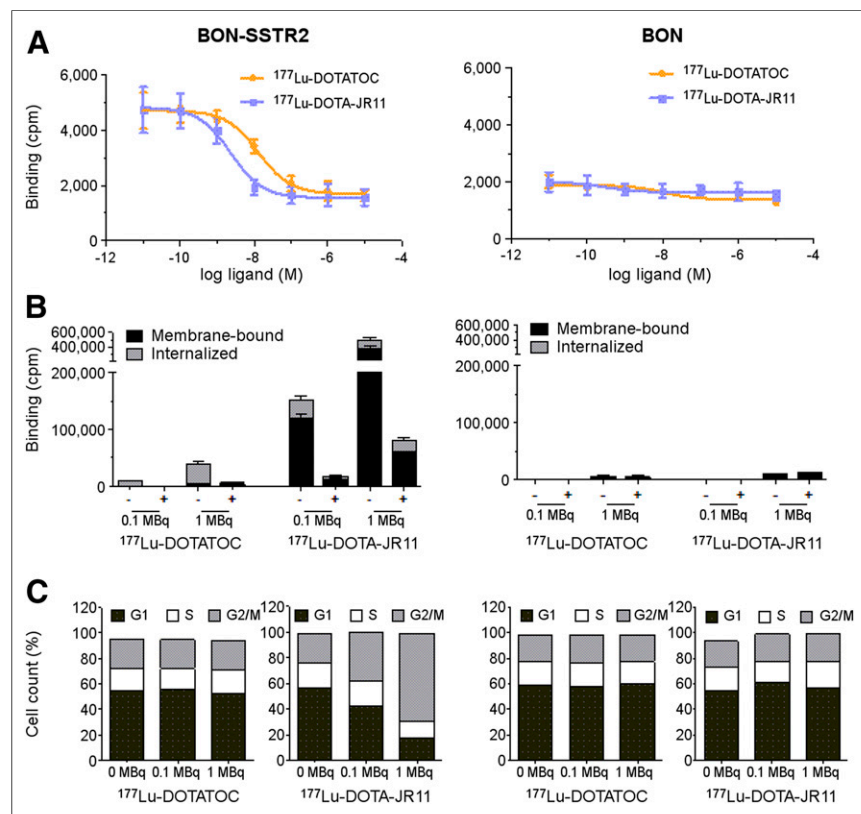


FIGURE 1. (A) SSTR2-transfected and native BON cells were incubated with ¹²⁵I-labeled Tyr₁₁-somatostatin-14 and increasing concentrations of unlabeled DOTATOC or DOTA-JR11 (±SEM; *n* = 3 each). (B) Respective cell lines were incubated with different doses of ¹⁷⁷Lu-DOTATOC or ¹⁷⁷Lu-DOTA-JR11. Resulting membrane-bound and internalized fractions in absence (–) or presence (+) of 1 μM unlabeled octreotide are presented (mean ± SEM; *n* = 2–3). (C) Cell-cycle distribution is shown, depicting percentage of cells in each phase (*n* = 1). cpm = counts per minute.

In Vivo Imaging

For both ¹⁷⁷Lu-DOTATOC- and ¹⁷⁷Lu-DOTA-JR11-treated animals, growth was significantly different from the saline treatment group on day 20 (*P* < 0.001) and day 35 (*P* < 0.001). After the first treatment cycle with ¹⁷⁷Lu-DOTA-JR11, tumors showed a continuous decrease in size for 27 d (interquartile range [IQR], 20–56). In ¹⁷⁷Lu-DOTATOC-treated animals, tumors showed a decreased growth rate but no decrease in volume (Fig. 2A). One of the 4 animals in the ¹⁷⁷Lu-DOTA-JR11 group died unexpectedly after 111 d (tumor size, 125 mm³) and was withdrawn from the growth curve.

Kaplan–Meyer analysis (Fig. 2B) revealed the longest survival and growth delay for ¹⁷⁷Lu-DOTA-JR11-treated animals (Table 1).

Visual assessment of the T2-weighted MR images revealed increasing fractions of nonviable (hypointense) tumor tissue over time in all 3 groups (Fig. 3A). After the second PRRT cycle, ¹⁷⁷Lu-DOTATOC-treated tumors showed no relevant changes in morphology but, rather, remained in a stable state. In contrast, ¹⁷⁷Lu-DOTA-JR11-treated animals revealed a significant loss of overall tumor mass, with almost no viable tumor tissue 3 wk after PRRT. Subsequently, regrowth occurred in all treatment groups and was pronounced at the tumor rim. To confirm glucose metabolism as a biomarker for viability of the regrowing tissue, ¹⁸F-FDG PET was performed once tumors

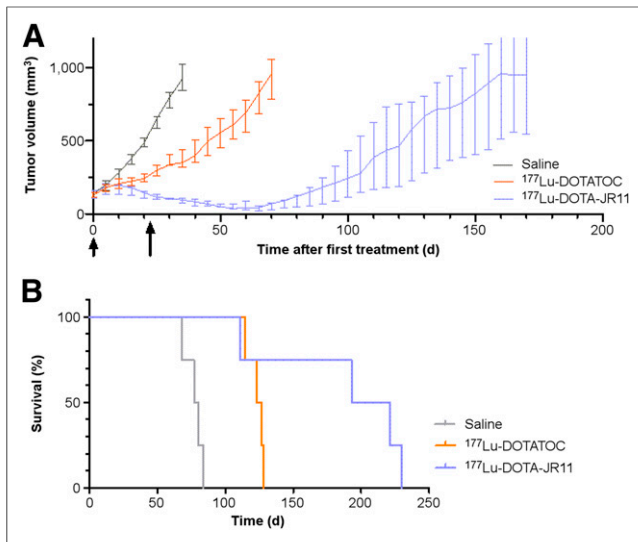


FIGURE 2. In vivo data of orthotopic pancreatic SSTR2-positive NEN model. (A) PRRT at 3-wk intervals (2 cycles): animals received 2 injections (arrows) of 100 μ L of saline ($n = 4$), 30 MBq of ^{177}Lu -DOTATOC ($n = 4$), or 20 MBq of ^{177}Lu -DOTA-JR11 ($n = 4$). Tumor growth was monitored until tumors reached volume of 1,000 mm^3 or animals dropped out for other reasons. (B) Corresponding Kaplan–Meyer survival curves.

reached at least 700 mm^3 . PET analysis showed that the hyperintense tumor areas related to metabolically active tissue, revealing a median viable tumor volume of 24.1% (IQR, 16–40) for ^{177}Lu -DOTATOC and 6.2% (IQR, 2–23) for ^{177}Lu -DOTA-JR11 after the second therapy cycle (Figs. 3B and 3C). The control group showed the largest fraction of viable tumor tissue in ^{18}F -FDG PET analysis (median, 46.4%; IQR, 35–56). Postmortem hematoxylin and eosin staining confirmed varying amounts of necrotic tissue between the tumor center and the tumor rim (Fig. 4A), showing more viable tissue at the rim.

SPECT/CT imaging 24 h after each therapy cycle showed a 4- to 6-fold higher median tumor uptake, as well as a 3- to 5-fold higher tumor-to-kidney ratio, for ^{177}Lu -DOTA-JR11 than for the SSTR agonist DOTATOC (Supplemental Fig. 2). Although ^{177}Lu -DOTATOC showed decreased uptake during the second cycle ($P = 0.01$), descriptive data indicate an increasing uptake for ^{177}Lu -DOTA-JR11 ($P = 0.1$). Kidney uptake did not significantly differ between treatment groups or therapy cycles (Table 2).

DISCUSSION

PRRT with the receptor agonist ^{177}Lu -DOTATATE is a standard treatment regimen approved by the Food and Drug Administration

TABLE 1
Median Survival and Growth Delay

Treatment group	Survival (d)	Growth delay* (d)
Saline	80 (72–84)	—
^{177}Lu -DOTATOC	126 (118–129)	46 (38–49)
^{177}Lu -DOTA-JR11	207 (132–228)	141 (113–150)

*Compared with saline-treated animals.
Data in parentheses are IQR.

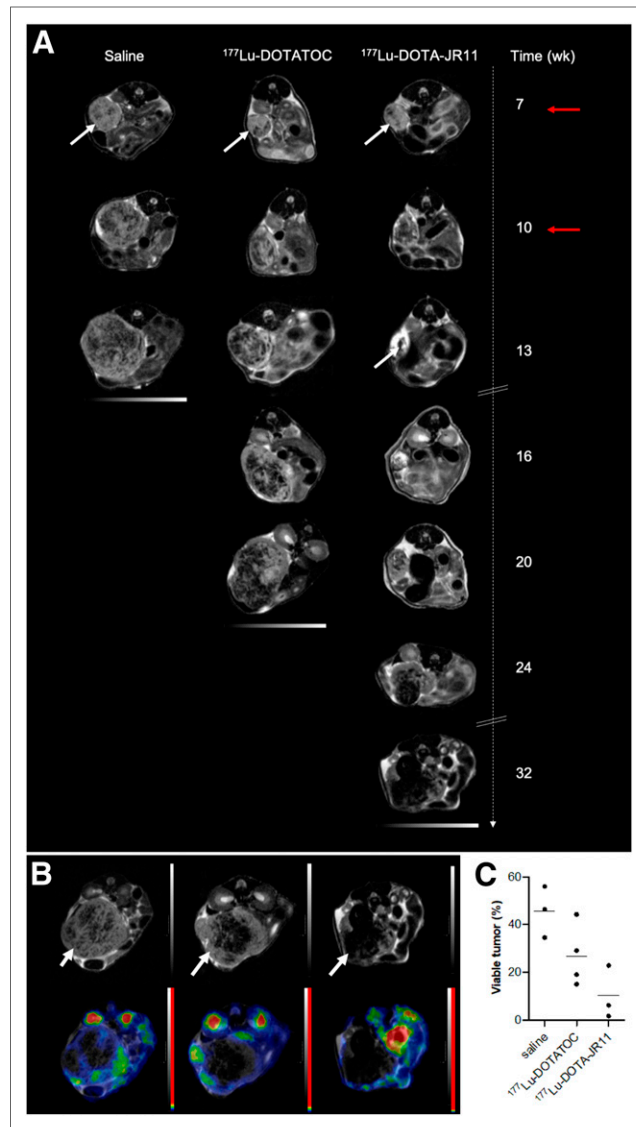


FIGURE 3. Tumor tissue monitoring over time. (A) Representative axial T2-weighted MRI of orthotopic tumors (white arrows) for different treatment regimens. Animals received 2 injections (red arrows) of 100 μ L of saline, 30 MBq of ^{177}Lu -DOTATOC, or 20 MBq of ^{177}Lu -DOTA-JR11. Tumor tissue appears rather hyperintense, whereas increasing portion of nonviable (e.g., necrotic) tissue appears hypointense. (B) Corresponding T2-weighted MRI (upper row) and ^{18}F -FDG PET/MRI (lower row); metabolically active regions are seen within tumor. (C) Dot plot representing viable tumor volume and mean values (horizontal line).

and the European Medicines Agency for patients with metastatic NENs. Novel SSTR antagonists such as ^{177}Lu -DOTA-JR11 have recently shown potential benefit over SSTR agonists for PRRT. In this study, we analyzed the morphologic and metabolic treatment efficacy of 2 subsequent PRRT cycles with the SSTR antagonist ^{177}Lu -DOTA-JR11, in comparison to the receptor agonist ^{177}Lu -DOTATOC, over time in an orthotopic NEN tumor mouse model by SPECT, PET, and MRI.

Although the antagonist DOTA-JR11 showed a much lower internalization rate of only 20% of the cell-bound activity in vitro, and thus a higher radiation distance to the nucleus, ^{177}Lu -DOTA-JR11 caused an activity-dependent increase in tumor cell

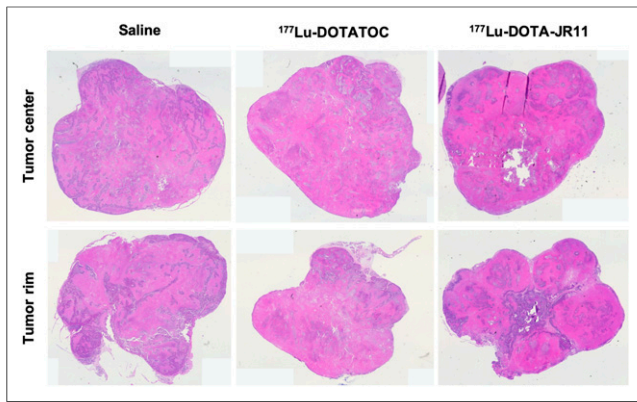


FIGURE 4. Immunohistochemistry of tumor tissue cross sections: Hematoxylin and eosin staining shows different amounts of necrosis between tumor rim and center.

accumulation in the G2/M phase and a decreased fraction of cells in the G0/G1 phase, compared with the control group, whereas the same amount of radioactivity of ^{177}Lu -DOTATOC did not affect the cell cycle. A possible explanation for this interesting and clinically relevant observation is that, compared with DOTATOC, the antagonistic ligand DOTA-JR11 revealed a 6-fold higher affinity for SSTR and a 10-fold higher activity bound to BON-SSTR2 tumor cells, resulting in a measurable, favorable therapeutic effect of G2/M cell-cycle arrest (Fig. 1). These promising data are in line with previously published results on SSTR2-transfected U2OS cells by Dalm et al., who reported an increased number of DNA double-strand breaks for antagonists (9).

In vivo, a significant reduction in tumor volume was observed only after ^{177}Lu -DOTA-JR11 treatment (Fig. 2A). This observation is partially in line with the findings of Dalm et al., who reported a decrease in tumor size for both radiopharmaceuticals, with a greater decrease in SSTR antagonist-treated animals (9). Additionally, we found increasing fractions of hypointense tissue within the tumors (Fig. 3A), most likely consisting of necrotic or apoptotic cells (20). As such effects are seen in all treatment groups, a possible explanation is the fast growth rate of the tumors and, thus, a consequent lack of center perfusion. Since central necrosis is more pronounced in PRRT-treated tumors and regrowth was observed primarily at the rim, relatively higher radiation doses in the tumor center, as described by Champion et al. (21), may also play a role in explaining our observation.

This effect was particularly pronounced in ^{177}Lu -DOTA-JR11-treated animals, and correlating ^{18}F -FDG PET images revealed the least amount of metabolically active tumor tissue (Fig. 3B and 3C). Hence, these findings indicate—in addition to the overall reduction in tumor mass—a greater destruction of viable tumor tissue by ^{177}Lu -

DOTA-JR11, independent of the apparent tumor size. Tumor volume reduction, such as by chemotherapy or PRRT, is a valuable tool to prepare advanced but potentially resectable NENs for curative surgery (22). The more pronounced and distinct cytoreductive effect of ^{177}Lu -DOTA-JR11, in comparison to ^{177}Lu -DOTATOC, may therefore be of great interest for using PRRT as a neoadjuvant tool in NEN therapy.

The growth delay in our study was significantly longer than previously reported (9). This difference may be explained by various factors, the first being a second therapy cycle. Baum et al. reported longer progression-free survival for patients receiving more than 1 PRRT cycle of ^{177}Lu -DOTATOC (23). A second factor is the lower number of cells injected in our study ($2\text{--}2.2 \times 10^6$ vs. $4\text{--}40 \times 10^6$), resulting in an overall reduced pace of tumor growth. A third factor is the difference in growth curves between the SCLC cell line H69 and the SSTR2-transfected BON cells. Finally, a fourth factor is the difference in tumor location (orthotopic vs. subcutaneous). Orthotopic tumor models are known to present a different physiology, such as higher vascular density and perfusion (24). These characteristics make the tumor more accessible to drugs and may translate into a longer delay in tumor growth.

Tumor and kidney uptake of the respective radiopharmaceuticals was monitored by SPECT imaging during each therapy cycle. Although the uptake of ^{177}Lu -DOTA-JR11 remained stable or even increased over the course of 2 PRRT cycles, ^{177}Lu -DOTATOC uptake significantly decreased (Table 2), and although kidney uptake was not different during the second treatment cycle, an increased tumor-to-kidney ratio was calculated for ^{177}Lu -DOTA-JR11 for the second treatment cycle. In comparison, the tumor-to-kidney ratio in the ^{177}Lu -DOTATOC group decreased (Supplemental Fig. 2). Since renal failure is an important therapy-limiting factor (25), high tumor-to-kidney ratios are favorable to successfully treat tumors without major kidney toxicity. Wild et al. reported a 6.2-fold higher tumor-to-kidney ratio for the SSTR antagonist ^{177}Lu -DOTA-JR11 than for ^{177}Lu -DOTATATE in a clinical trial (7). The overall lower tumor-to-kidney ratios reported in our study may result from the lack of nephroprotection. Beykan et al. found a 2-fold increased kidney uptake of ^{177}Lu -DOTA-JR11 when no renal protection was applied (10). It must be mentioned, though, that DOTATATE and DOTATOC have different SSTR2 affinities in vitro and, thus, are not directly comparable. Nevertheless, the data presented here confirm the favorable role of ^{177}Lu -DOTA-JR11 in reducing renal radiation exposure during PRRT in NENs.

In our preliminary study, all animals died after administration of 30 MBq of ^{177}Lu -DOTA-JR11; thus, the activity was reduced by 30%. Because bone marrow is also thought to be a therapy-limiting factor (8), a possible explanation is a hematotoxic effect. Reidy-Lagunes et al. reported increased grade 4 hematologic

TABLE 2
Median Uptake of ^{177}Lu -DOTATOC and ^{177}Lu -DOTA-JR11 24 Hours After Injection

Treatment group	First PRRT cycle		Second PRRT cycle	
	Tumor	Kidney	Tumor	Kidney
^{177}Lu -DOTATOC	2.7 (2.4–2.9)	2.6 (2.0–2.7)	2.0 (1.8–2.3)	2.5 (2.3–4.2)
^{177}Lu -DOTA-JR11	10.4 (9.3–10.9)	3.2 (2.8–3.6)	12.9 (9.9–14.0)	3.0 (2.9–3.5)

Data are percentage injected activity per milliliter, followed by IQR in parentheses.

toxicity after 1 and 2 PRRT cycles using ^{177}Lu -satoreotide tetraxetan (JR11); after reducing the amount of ^{177}Lu by 50%, no patients developed hematotoxicity (12). Even though we cannot retrospectively evaluate the reason for premature death in the animals in our preliminary study, as we did not take blood samples, the administered activity in future studies and the respective toxic effects to organs should be evaluated carefully.

One limiting factor of the present study was the small sample size. Because multimodal imaging is time-consuming and because of restricted tracer availability, we had to limit the number of animals and imaging sessions to guarantee the feasibility of such a long-term study.

CONCLUSION

We showed a pronounced cytotoxic treatment effect for the SSTR antagonist ^{177}Lu -DOTA-JR11 in comparison to the standard agonistic ^{177}Lu -DOTATOC, leading to a significant reduction in viable tumor tissue, a more pronounced delay in tumor growth, and a longer survival in vivo, as well as a higher accumulation of cells in the vulnerable G2/M cell-cycle phase in vitro. Over the course of 2 PRRT cycles, SPECT/CT imaging revealed an approximately 4-fold higher tumor uptake, which remained high during the second cycle of treatment, as well as a more favorable tumor-to-kidney ratio than was obtained with ^{177}Lu -DOTATOC.

DISCLOSURE

This work was supported in part by Technologiestiftung Berlin (TSB) for NanoSPECT/CT Plus use, by Deutsche Forschungsgemeinschaft (DFG) for nanoScan PET/MRI (INST 335/454-1 FUGG) use, and by SFB1340 TPB06 to Anja Kühl. No other potential conflict of interest relevant to this article was reported.

ACKNOWLEDGMENTS

We thank Janpeter Hirsch for assisting with data processing, Fränze Schmidt for helping with PET/MRI measurements, Dietrich Polenz for establishing the animal model, Prof. Helmut Maecke (University Hospital Freiburg, Germany) for providing the precursor DOTA-JR11, and Prof. Courtney M. Townsend, Jr. (University of Texas, Galveston), for providing the human pancreatic BON cells.

KEY POINTS

QUESTION: Compared with ^{177}Lu -DOTATOC, does ^{177}Lu -DOTA-JR11 show favorable treatment effects for PRRT in NENs?

PERTINENT FINDINGS: In an orthotopic mouse model, ^{177}Lu -DOTA-JR11 showed a higher therapeutic effect and a more favorable tumor-to-kidney ratio.

IMPLICATIONS FOR PATIENT CARE: ^{177}Lu -DOTA-JR11 is a promising radiopharmaceutical for advanced NENs.

REFERENCES

1. Pavel M, O'Toole D, Costa F, et al. ENETS consensus guidelines update for the management of distant metastatic disease of intestinal, pancreatic, bronchial neuroendocrine neoplasms (NEN) and NEN of unknown primary site. *Neuroendocrinology*. 2016;103:172–185.
2. Falconi M, Eriksson B, Kaltsas G, et al. ENETS consensus guidelines update for the management of patients with functional pancreatic neuroendocrine tumors and non-functional pancreatic neuroendocrine tumors. *Neuroendocrinology*. 2016;103:153–171.
3. Strosberg J, El-Haddad G, Wolin E, et al. Phase 3 trial of ^{177}Lu -dotatate for midgut neuroendocrine tumors. *N Engl J Med*. 2017;376:125–135.
4. Ginj M, Zhang H, Waser B, et al. Radiolabeled somatostatin receptor antagonists are preferable to agonists for in vivo peptide receptor targeting of tumors. *Proc Natl Acad Sci USA*. 2006;103:16436–16441.
5. Fani M, Braun F, Waser B, et al. Unexpected sensitivity of sst2 antagonists to N-terminal radiometal modifications. *J Nucl Med*. 2012;53:1481–1489.
6. Wild D, Fani M, Behe M, et al. First clinical evidence that imaging with somatostatin receptor antagonists is feasible. *J Nucl Med*. 2011;52:1412–1417.
7. Wild D, Fani M, Fischer R, et al. Comparison of somatostatin receptor agonist and antagonist for peptide receptor radionuclide therapy: a pilot study. *J Nucl Med*. 2014;55:1248–1252.
8. Nicolas GP, Mansi R, McDougall L, et al. Biodistribution, pharmacokinetics, and dosimetry of ^{177}Lu -, ^{90}Y -, and ^{111}In -labeled somatostatin receptor antagonist OPS201 in comparison to the agonist ^{177}Lu -DOTATATE: the mass effect. *J Nucl Med*. 2017;58:1435–1441.
9. Dalm SU, Nonnekens J, Doeswijk GN, et al. Comparison of the therapeutic response to treatment with a ^{177}Lu -labeled somatostatin receptor agonist and antagonist in preclinical models. *J Nucl Med*. 2016;57:260–265.
10. Beykan S, Dam JS, Eberlein U, et al. ^{177}Lu -OPS201 targeting somatostatin receptors: in vivo biodistribution and dosimetry in a pig model. *EJNMMI Res*. 2016;6:50.
11. Beykan S, Fani M, Jensen SB, et al. In vivo biokinetics of ^{177}Lu -OPS201 in mice and pigs as a model for predicting human dosimetry. *Contrast Media Mol Imaging*. 2019;2019:6438196.
12. Reidy-Lagunes D, Pandit-Taskar N, O'Donoghue JA, et al. Phase I trial of well-differentiated neuroendocrine tumors (NETs) with radiolabeled somatostatin antagonist ^{177}Lu -satoreotide tetraxetan. *Clin Cancer Res*. 2019;25:6939–6947.
13. Exner S, Prasad V, Wiedenmann B, Grotzinger C. Octreotide does not inhibit proliferation in five neuroendocrine tumor cell lines. *Front Endocrinol (Lausanne)*. 2018;9:146.
14. Erdmann S, Niederstadt L, Koziol EJ, et al. CMKLR1-targeting peptide tracers for PET/MR imaging of breast cancer. *Theranostics*. 2019;9:6719–6733.
15. Albrecht J, Polenz D, Kuhl AA, et al. Diffusion-weighted magnetic resonance imaging using a preclinical 1 T PET/MRI in healthy and tumor-bearing rats. *EJNMMI Res*. 2019;9:21.
16. Erben U, Lodenkemper C, Spieckermann S, Heimesaat MM, Siegmund B, Kühl AA. Histomorphology of intestinal inflammation in inflammatory bowel diseases (IBD) mouse models and its relevance for IBD in men. *Int J Clin Exp Pathol*. 2016;9:408–442.
17. Friedrich S, Brunner E, Pauly M. Permuting longitudinal data in spite of the dependencies. *J Multivariate Anal*. 2017;153:255–265.
18. Friedrich S, Konietzschke F, Pauly M. Analysis of multivariate data and repeated measures designs with the R package MANOVA.RM. arXiv.org website. <https://arxiv.org/abs/1801.08002>. Published January 24, 2018. Accessed November 5, 2020.
19. Noguchi K, Gel Y, Brunner E, Konietzschke F. nparLD: an R software package for the nonparametric analysis of longitudinal data in factorial experiments. *J Stat Softw*. 2012;50.
20. Jardim-Perassi BV, Huang S, Dominguez-Viqueira W, et al. Multiparametric MRI and coregistered histology identify tumor habitats in breast cancer mouse models. *Cancer Res*. 2019;79:3952–3964.
21. Champion C, Zanotti-Fregonara P, Hindie E. CELLDOSE: a Monte Carlo code to assess electron dose distribution—S values for ^{131}I in spheres of various sizes. *J Nucl Med*. 2008;49:151–157.
22. Pozzari M, Maisonneuve P, Spada F, et al. Systemic therapies in patients with advanced well-differentiated pancreatic neuroendocrine tumors (PanNETs): when cytoreduction is the aim—a critical review with meta-analysis. *Cancer Treat Rev*. 2018;71:39–46.
23. Baum RP, Kluge AW, Kulkarni H, et al. [^{177}Lu -DOTA] 0 -D-Phe 1 -Tyr 3 -octreotide (^{177}Lu -DOTATOC) for peptide receptor radiotherapy in patients with advanced neuroendocrine tumours: a phase-II study. *Theranostics*. 2016;6:501–510.
24. Ho KS, Poon PC, Owen SC, Shoichet MS. Blood vessel hyperpermeability and pathophysiology in human tumour xenograft models of breast cancer: a comparison of ectopic and orthotopic tumours. *BMC Cancer*. 2012;12:579.
25. van Essen M, Krenning EP, Kam BL, de Jong M, Valkema R, Kwekkeboom DJ. Peptide-receptor radionuclide therapy for endocrine tumors. *Nat Rev Endocrinol*. 2009;5:382–393.